Solar Phys (2019) 294:177
https://doi.org/10.1007/s11207-019-1569-5

Meteospace, a New Instrument for Solar Survey at the Calern Observatory

J.-M. Malherbe[1,2] · Th. Corbard[3] · K. Dalmasse[4] · The Meteospace team[5]

Received: 15 August 2019 / Accepted: 7 December 2019 / Published online: 19 December 2019

Abstract High-cadence observations of solar activity (active regions, flares, filaments) in the Hα line were performed at Meudon and Haute Provence Observatories from 1956 to 2004. More than 7 million images were recorded, mainly on 35 mm films. After a review of the scientific interest of solar surveys at high temporal resolution and the historical background, we describe the new instrument which will operate automatically in 2020 at the Calern station of the Côte d'Azur observatory (1270 m). It will replace the former heliographs with improved cadence, seeing and time coverage. We summarize the capabilities of the optical design and present new scientific perspectives in terms of flare onset and Moreton wave detection.

Keywords Chromosphere · Full-sun · Flares · Active regions · Filaments · Moreton waves · Heliograph

Electronic supplementary material The online version of this article (https://doi.org/10.1007/s11207-019-1569-5) contains supplementary material, which is available to authorized users.

✉ J.-M. Malherbe
Jean-Marie.Malherbe@obspm.fr

Th. Corbard
Thierry.Corbard@oca.eu

K. Dalmasse
Kevin.Dalmasse@irap.omp.eu

The Meteospace team
url: http://www.obspm.fr

1 LESIA, Observatoire de Paris, 92195 Meudon, France

2 PSL Research University, Paris, France

3 Université Côte d'Azur, Observatoire de la Côte d'Azur, CNRS, Laboratoire Lagrange, 06304 Nice, France

4 IRAP, Université de Toulouse, CNRS, CNES, UPS, 31028 Toulouse, France

5 Observatoires de Paris et de la Côte d'Azur, France

1. Introduction

Systematic observations of the full solar disk started at the Meudon Observatory in 1908 with Deslandres spectroheliograph (Malherbe and Dalmasse, 2019). Spectroheliograms are obtained by spectroscopic scans of the Sun, producing line profiles and narrow bandpass images at constant wavelength. This is a low cadence instrument dedicated to the study of long term solar activity.

In addition several heliographs performed high cadence (60 seconds) Hα observations from 1956 to 2004 at Meudon and Haute Provence (OHP) observatories, which produced more than 7 million images. This survey of fast solar activity (flares, evolution of active regions and filaments) was based on Lyot filters and started in the frame of the International Geophysical Year (IGY 1957). Unfortunately, only 10% of the collection is digitized, the oldest part being on films. Nowadays, such observations are mainly done with narrow band imagers such as Fabry–Pérot filters (*e.g.* Global Oscillation Network Group (GONG) Hα network: Harvey *et al.*, 2011), but some Lyot filters remain in activity (*e.g.* Global Hα Network (GHN): Gallagher *et al.*, 2002).

This work is intended to promote high-cadence observations of the Sun in the context of space weather monitoring. Section 2 recalls the scientific interest of such observations. In Section 3, we present the historical background summarizing the evolutions and main discoveries of the Meudon and OHP heliographs (1956–2004). Section 4 describes the new instrument which is going to replace them at Calern observatory. Section 5 discusses new perspectives in terms of flare onset and Moreton waves detection.

2. Scientific Goal of High Cadence Observations

Solar flares and coronal mass ejections (CMEs) are energetic events associated with the sudden release of magnetic energy in response to the development of resistive (Furth, Killeen, and Rosenbluth, 1963; Antiochos, DeVore, and Klimchuk, 1999) or ideal (Amari and Luciani, 1999; Kliem and Török, 2006) MHD instabilities in the coronal magnetic field. During these events, typically $10^{28} - 10^{33}$ erg of magnetic energy are released in about $10^3 - 10^4$ s (Shibata and Magara, 2011). The energy is released by magnetic reconnection and converted into thermal, kinetic and radiated energy (Carmichael, 1964; Sturrock, 1966; Hirayama, 1974; Kopp and Pneuman, 1976). Through particle acceleration and ejections, flares and CMEs are the two major drivers of space weather that can cause various environmental hazards at the Earth (Schrijver *et al.*, 2012), and for which high-cadence observations of the Sun are required.

Hα is the best line for fast imaging of chromospheric structures such as filaments, which are cool and dense material that appear as elongated and dark structures. They are formed of chromospheric plasma confined in highly stressed coronal magnetic fields that overlay polarity inversion lines (Aulanier and Démoulin, 1998; Schmieder *et al.*, 2006). Filaments are typical precursors of flares, including confined flares associated with failed filament eruption (Török and Kliem, 2005) and flares for which the filament erupts and leads to the formation of a CME (Moore *et al.*, 2001). In the latter case, the filament is usually characterized by a slow rise (taking hours) until it reaches a critical height beyond which the system becomes unstable and the filament erupts (Kahler *et al.*, 1988; Sterling and Moore, 2005). In this regard, high-cadence observations of filaments are needed for near real-time prediction of their ejection.

Hα imaging also provides observations of flare ribbons, a useful signature for real-time detection of flares for which there is either no filament eruption (Dalmasse *et al.*, 2015) or no filament at all (Masson *et al.*, 2009). Flare ribbons are surface brightenings that can be observed in ultraviolet (UV) and Hα (Schmieder *et al.*, 1987). They are caused by the interaction of energetic particles and thermal energy (produced at the reconnection region) with the lower and denser atmospheric layers (review by Fletcher *et al.*, 2011). The spatio-temporal evolution of Hα ribbons provides information on the flare dynamics. If one further combines Hα data with photospheric magnetograms and some sort of modeling, it is then possible to derive the reconnection rate (Forbes and Priest, 1984; Qiu *et al.*, 2002), the energy release rate (Asai *et al.*, 2004; Isobe, Takasaki, and Shibata, 2005), and the flare energy (Toriumi *et al.*, 2017).

Moreton waves are another flare-related signature for which high-cadence imaging is required. They are large-scale disturbances propagating in the solar atmosphere in Hα observations (Moreton, 1960). They materialize as arc-shaped, bright fronts in the center and blue wing of the Hα line, which propagate out to distances of up to 600 Mm in the extreme cases (review by Warmuth, 2015). Their typical propagation speed is in the range $400-2500$ km s^{-1} (Narukage *et al.*, 2002; Muhr *et al.*, 2010; Liu *et al.*, 2013). The speed and signature argue in favour of a chromospheric counterpart of a coronal perturbation that compresses and pushes the chromosphere downwards (Uchida, 1968). Coronal waves were detected by the Extreme ultraviolet Imager Telescope (EIT) onboard SOHO (Klassen *et al.*, 2000) and later by the Atmospheric Imaging Assembly (AIA) onboard SDO (Nitta *et al.*, 2013), with better temporal and spatial resolution. Their physical nature (CME-driven or freely propagating MHD shock-wave) is not yet fully understood.

Moreton waves can disturb the ambient coronal magnetic field and remote filaments, and seem to be associated with strongest flare or CME events (Warmuth, 2015), which are more likely to be very geo-effective. Moreton waves detection at high cadence, by running- or base-difference Hα imaging of the chromosphere (Section 5), should allow one to identify in real-time the potentially most energetic and dangerous eruptive events in space weather applications.

In this context, the new instrument presented here has two major goals:

i) solar activity monitoring in chromospheric lines as Hα center (flares and filaments) and CaII K (magnetic proxy);
ii) flare, CME onset and Moreton wave detection using two high cadence (15 seconds) Hα filters (center and blue wing).

3. Historical Background of the French Heliographs

More than 7 million images were produced both at Meudon and OHP between 1956 and 2004 in the context of high-cadence (60 seconds) observations to investigate solar activity events (Table 1 and Figure 4).

The story began with the invention of the monochromatic birefringent filter by Lyot (1944). The first Hα heliograph was built by Grenat and Laborde (1954). Systematic observations started in 1956 with 35 mm films (Figure 1). The 45 meters long films (Kodak Technical Pan TP2415) recorded each 2200 full Sun images, 15 mm diameter and 0.75 Å FWHM. The film resolution (better than 125 lines/mm or less than $1''$ at the Sun) was limited by the seeing ($2''$ typical). A similar instrument started at OHP in 1958 and worked

Table 1 1956-2004 Hα observations at Meudon and OHP (FS = full Sun; PS = part Sun). Three wavelengths mean that line center, blue and red wings ($\pm$0.75 Å) are observed in sequence, while for five wavelengths, we have four wing positions ($\pm$1.0 Å, $\pm$0.5 Å).

Site	Date	Wavelength number	Sun diameter [mm]	Resolution [arcsec]	FWHM Å
Meudon (films)	1956–1960	1	15 (FS)	1.0	0.75
	1965–1982	1	11 (FS)	1.4	0.75
	1965–1984	3	35 (PS)	0.5	0.75
	1983–1984	1	16 (FS)	1.0	0.75
	1985–1997	3 or 5	21 (FS)	0.8	0.50
Meudon (CCD)	1999–2004	3	8.5 (FS)	3.7	0.50
OHP (films)	1958–1995	1	15 (FS)	1.0	0.75

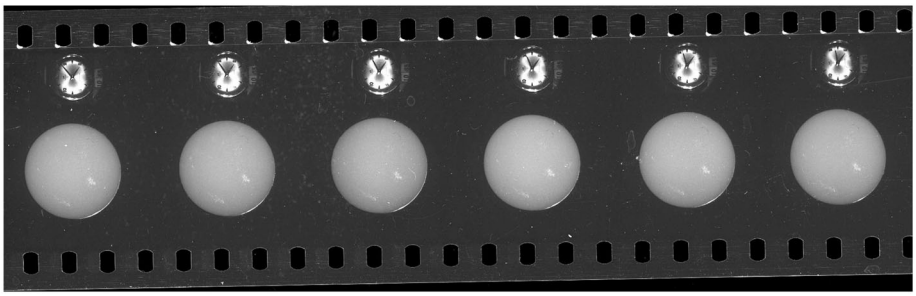

Figure 1 Example of 11 mm Hα monochromatic full Sun images got with Meudon heliograph between 1965 and 1985, 0.75 Å FWHM (4 October 1965 from 16:08 to 16:13 UT).

until 1995, producing 2.6 million images. The pair of sites allowed for an increase in temporal coverage, as clear sky at OHP is more frequent. The 1957 IGY motivated the scientific program of both instruments.

Between 1960 and 1965, Meudon observations were interrupted but continued at OHP. A new three-wavelength instrument was built for observations at Hα center, blue and red wings ($\pm$0.75 Å) using a three-stage tunable Lyot filter with motorized rotating plates (Figure 2, Michard, 1965, Demarcq *et al.*, 1985). Observations started in 1965, covering about 30% of the solar area (16 $\times$ 20 mm FOV selected in the 35 mm image of the Sun). For that reason, a second routine, full disk and only at Hα center, started at the same time (11 mm solar diameter). Both instruments had 0.75 Å FWHM and were in production until 1984.

In 1985, a new tunable Lyot filter, with better performance (Hα center, blue and red wings ($\pm$0.50 Å, $\pm$1.0 Å, 0.50 Å FWHM) was developed (Figure 3, Demarcq *et al.*, 1985). It was mounted between two lenses of 360 mm focal length; this afocal system was fed by a 150/2250 mm telescope. Observers chose three or five wavelengths according to solar activity level, plus a long exposure image for prominences at line center. This five-stage Lyot filter (11 Å distance between maxima) was optimized to cut secondary lobes. The Hα peak was isolated by a three cavity 3.5 Å FWHM blocking filter. This device provided full disk images (21 mm diameter), such that the old 11 mm Hα center routine was stopped. A 1536 $\times$ 1024 cooled CCD camera from Princeton Instruments, supporting a 140 mm objective, replaced the film in 1999 (9 μ pixel, 12 bits, cooled KAF1600 sensor), producing 0.7 million FITS images until 2004 (Table 1 shows that, contrarily to the film, CCD images

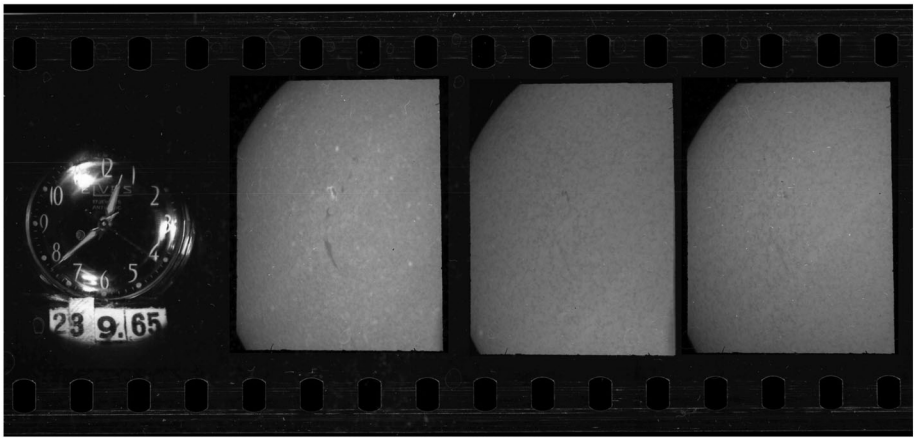

Figure 2 Example of three-wavelength Hα part Sun images got with Meudon heliograph between 1965 and 1984: line center, blue and red wings ($\pm$0.75 Å), 0.75 Å FWHM, here images of 4 October 1965 at 12:38 UT).

were undersampled). FITS data are off line (CD/DVD), but freely available upon request. Light curves and quick look MPEG movies are on line at the BASS2000 solar database (http://bass2000.obspm.fr/home.php?lang=en).

Figure 4 summarizes observations made between 1956 and 2004. About 6.5 million images have been recorded on 35 mm films (a total of 130 kilometers), and 0.7 million of CCD images are archived. The detailed list is available at: http://www.lesia.obspm.fr/perso/jean-marie-malherbe/heliograph/index.html

The cost makes impossible a systematic scan of the 3000 films of this exceptional collection, but films of interest can be digitized individually upon request (8 bits, 157 pixels/mm scans, sampling better than 1″/pixel, TIF format, one file for 100 mm of film).

Observations have been mainly used by the Meudon group and exploited qualitatively, as long as films were not digitized, to investigate chromospheric flares and filament instabilities. The multi-wavelength filters allowed one to study mass motions in active regions.

Concerning flares, Martres and Pick (1962) found a relationship with radio bursts observed in Nançay. Mouradian, Martres, and Soru-Escaut (1983) suggested that a flare is composed of several elementary eruptive phenomena in relation with magnetic emerging flux, involving the presence of both cold (the surging arch at 10^4 K) and hot (the flaring arch at 10^7 K) magnetic loops. Martres (1989) found evidence for homologous flaring. Mouradian *et al.* (1989) compared Hα features and X-ray brightenings at flare onset. Later with the digital version of the three-wavelength instrument, Pick *et al.* (2005) and Maia *et al.* (2003) investigated CMEs and flares using Hα and radio data.

As for filaments, Mouradian and Soru-Escaut (1989) discovered the existence of rigid rotation points (the pivot points) in some filaments which could play a role in instabilities. Soru-Escaut and Mouradian (1990) suggested that heating and cooling mechanisms could explain several cases of sudden disappearances and reappearances. Hence, Mouradian, Soru-Escaut, and Pojoga (1995) proposed two physical classes of disappearances, involving either thermal or dynamic processes.

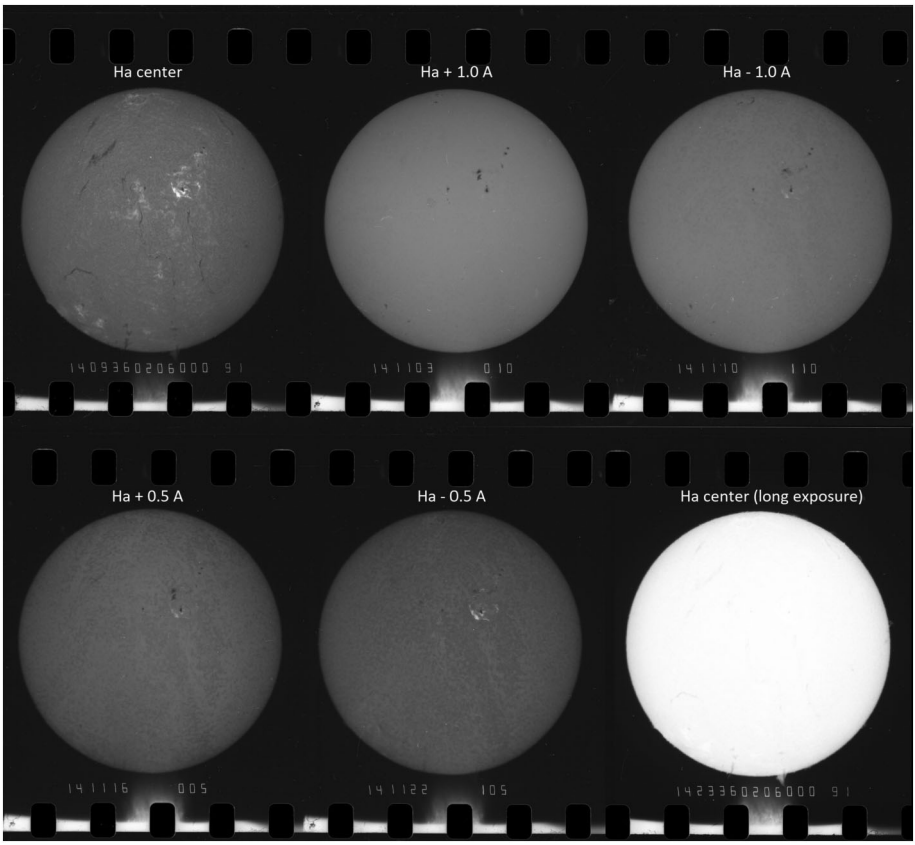

Figure 3 Example of five-wavelength Hα full Sun images got with Meudon heliograph between 1985 and 1997, line center, red and blue wings ($\pm$0.1 Å, $\pm$0.50 Å) and overexposed line core for prominences (0.50 Å FWHM, flare of 2 June 1991 at 14:11 UT).

Table 2 Optical design (the two Hα telescopes are identical, apart the filter).

Telescope	O1 [mm]	O2 [mm]	O3 [mm]	O4 [mm]	f_{equiv} [mm]	FOV [arcmin]
Hα	816	250	250	−50/+60	983	35
CaII K	820	−220	250		983	35

4. The New Heliograph

A small rolling house has been built at Calern observatory (1270 m elevation) in order to have better weather and seeing conditions than at Meudon or OHP. The equatorial mount was constructed by Valmeca. It supports the instruments which are enclosed in a $1.7 \times 0.5 \times 0.5$ m^3 box, thermally regulated above ambient temperature at 27° C by active heating and passive cooling.

The new instrument is composed of three telescopes (Tables 2 and 3) corresponding to the design of Figure 5. The two Hα telescopes are identical, except for the Fabry–Pérot etalons manufactured by DayStar corporation (professional series). The first filter is line

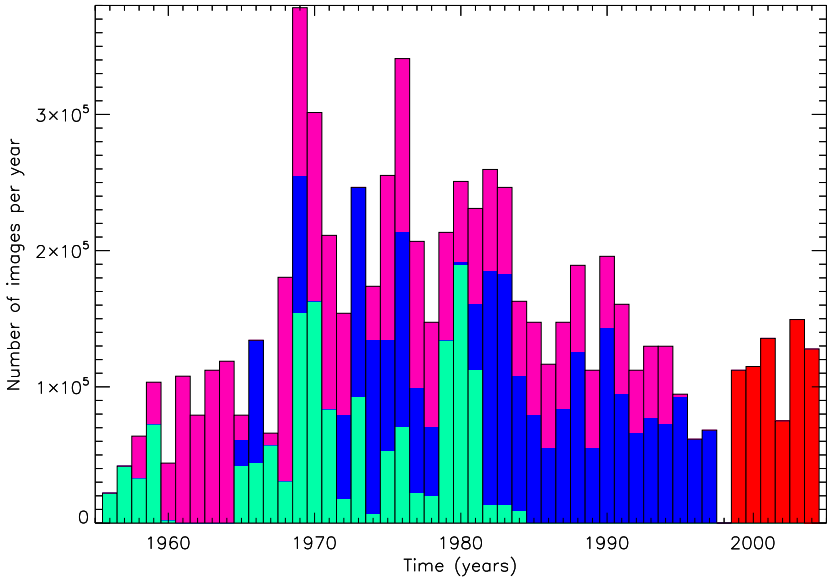

Figure 4 Number of Hα images got with Meudon and OHP heliographs between 1956 and 2004 (*green*: Meudon, 11 mm images; *pink*: Haute Provence, 15 mm images; *blue*: Meudon, three-wavelength (part Sun until 1985, full Sun after); *red*: Meudon, three-wavelength CCD full Sun).

Table 3 Filter characteristics.

Line	Wavelength (CWL) [Å]	FWHM (global) [Å]	Temperature [°C]	Peak distance [Å]	max. finesse	Blocking filter FWHM [Å]
Hα 1	6562.8	0.34	38	24.7	77	10.0
Hα 2	6562.3	0.46	65	19.7	61	8.6
CaII K	3933.7	1.5	23			

core centered, in order to observe active regions, flares and filaments. The second one is adjusted to the blue wing (choice discussed in Section 5). The third telescope is centered on CaII K with an interference filter from Barr company. The equivalent focal length is 983 mm providing a 9.13 mm solar image and 35′ FOV. Each detector (Table 4) is a 12 bits cooled camera from Quantum Scientific Imaging using shutterless interline CCD sensors from Sony (ICX694 and 814, respectively, for Hα and CaII K). The readout noise is 7 electrons RMS at 8 MHz. Exposure times are shorter than 10 ms.

Hα telescopes are afocal systems. O1 is the entrance objective (Takahashi TSA102, 102 mm diameter) protected in full aperture by a Baader energy rejection filter (ERF). The Fabry–Pérot etalon is located in the pupil image at F/30 between O2 and O3 (maximum beam aperture constrained by the manufacturer). O4 (a set of two separate lenses) is an amplifier and field corrector. A 80 mm diaphragm limits the optical resolution to 2.0″.

The calibration of the two Hα filters was done at F/60 with the high resolution spectrograph (R = 300000) of the Meudon solar tower. The surface filter (31.75 mm diameter) was scanned by the slit. Both filters exhibit 0.32 Å FWHM (homogeneous over the filter), but the

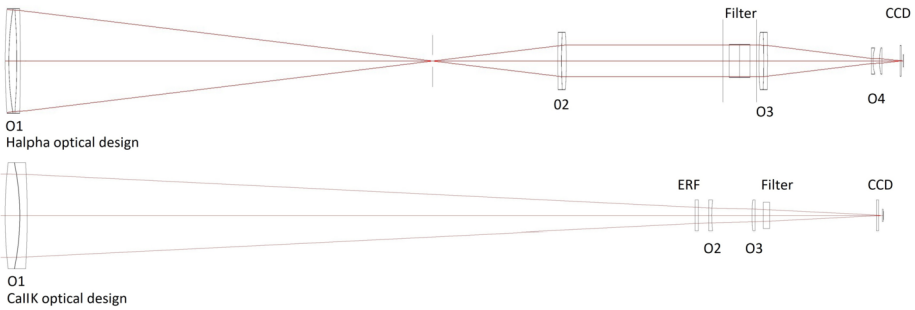

Figure 5 Optical design of the two Hα (*top*) and the CaII K (*bottom*) telescopes.

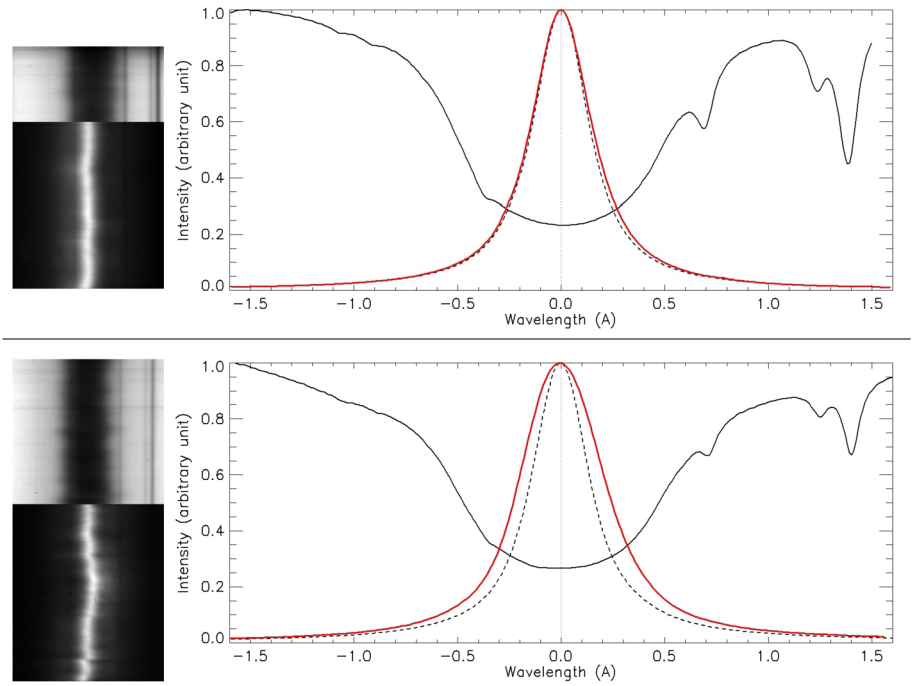

Figure 6 Calibration at F/60 of the two Hα filters (0.34 Å FWHM *top*, 0.46 Å FWHM *bottom*). *Left*: Hα observed line at disk center with or without the filter. *Right*: transmission functions; *black line*: observed line profile; *dashed line*: local typical transmission (0.32 Å FWHM); *red line*: global transmission averaged over the filter surface for pupil plane application.

scans show that the CWL varies from place to place. The pupil plane location of the afocal design allows one to correct this effect and delivers a uniform CWL image, but, as a counterpart, it increases the global FWHM (Figure 6). Hence, filter 1 (2019) is almost perfect (0.34 Å global FWHM) and is dedicated to Hα center images. Filter 2 (2009) has some optical defects (0.46 Å global FWHM) and is used for Hα wing (Moreton waves detection); it exhibits a 10% parasitic internal reflection which vanishes in the running-difference process (Section 5). Each Fabry–Pérot etalon is solid (mica spaced) and $\lambda/10$ surfaced. The Hα peak is selected by an internal 2-cavity 8-10 Å FWHM blocking filter. Adjacent peaks are about

Table 4 Detector characteristics.

Line	Dynamic range	Pixel [microns]	Sampling pixel [arcsec]	format [pixels]	Quantum efficiency [%]	Full well [ē]	Gain [ē/ADU]
Hα	2700	4.54	0.96	2758×2208	65	19000	0.40
CaII K	2570	3.69	0.78	3388×2712	60	18000	0.36

20 Å apart with only 0.34% transmission of the central peak. However, the blocking filter of etalon 2 is shifted by 2.8 Å. A colored longpass glass filter (RG630) suppresses short wavelengths (UV, blue, green), while IR radiation is rejected by a shortpass filter.

Both etalons are thermally regulated; the CWL is temperature dependent (9°C/Å typical). As the wavelength shift is very slow (about 0.1 Å/minute), contrarily to Lyot tunable filters based on rotating plates, it is not possible to scan line profiles, so that two filters are required for two wavelength positions (Figure 7).

The CaII K telescope provides a magnetic field proxy for active regions and faculae (Pevtsov *et al.*, 2016). As the filter is broad (1.5 Å FWHM), the design does not need to be afocal. O1 is the entrance objective (Takahashi FS102, 102 mm diameter). O2 and O3 constitute a focal amplifier. The 3934 Å filter is located close to the image plane and protected by an ERF. A 80 mm diaphragm limits the resolution to 1.25″.

Meteospace is an autonomous station: opening and closing the dome, weather control, catching the Sun, observations, data processing, real-time dissemination, database archiving: all operations are automated. Sensors permanently control the instrument and can decide to stop and close in case of cloud, rain, alarm or failure; alerts are sent to the local staff by a Short Message Service (SMS). The entry point to the data is the BASS2000 service, even if the full archive is physically located at Nice.

All data will be delivered freely to the solar community. Raw (level 0) data as well as standard processed data (level 1) will be available in real-time JPEG for quick look purpose and FITS for scientific use. Level 1 includes corrections as dark current, distortion and solar image rotation to present solar north up. The observing cadence is, respectively for Hα and CaII K, 15 and 60 seconds. The system will run systematically (weather permitted) under seeing conditions better than 2″ (sampling reported in Table 4). Following Thompson (2006), FITS headers include World Coordinates System (WCS) information concerning image pointing and orientation, allowing for the use of positioning tools.

5. New Perspectives for Flare Onset and Moreton Wave Detection

The purpose of the two high-cadence Hα telescopes is to improve the detection of flare onset and Moreton waves. Such events are suspected to be the counterpart of fast coronal EUV waves in the chromosphere, which could be compressed by the coronal shock above, producing $5-10$ km s^{-1} downflows (Warmuth, 2015).

We simulated the detection of Moreton waves by the 0.46 Å FWHM filter using the difference signal between a shifted profile and the quiet sun profile (Figure 8). We used the atlas profile from Delbouille, Roland, and Neven (1973) altered by 15% scattered light and shifted from -10 to $+10$ km s^{-1}. The filter CWL was moved from the blue to the red wing (-1.0 Å to $+1.0$ Å by 0.25 Å step). The best sensitivity is obtained, for chromospheric downflows, when the filter selects the blue wing (-0.5 Å, 9% and 17% enhancement respectively for 5 and 10 km s^{-1}). In the case of simultaneous up or downflows, both wings

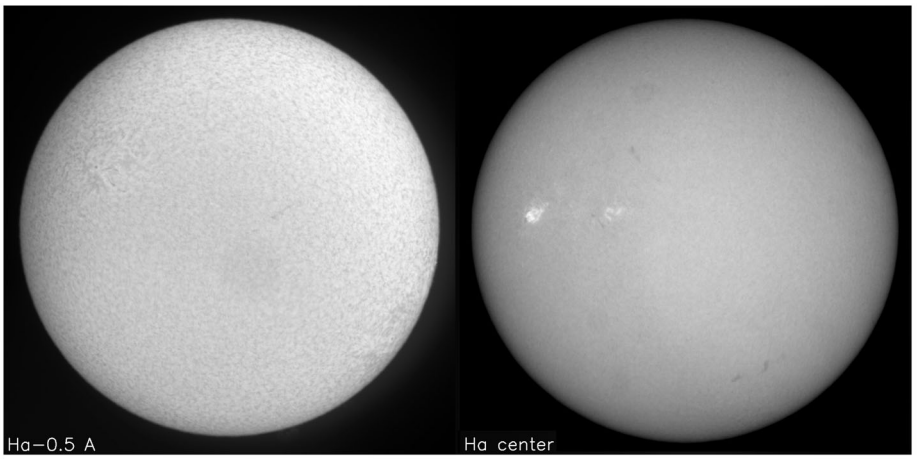

Figure 7 Images obtained with the 0.46 Å FWHM filter (29 August 2017) in Hα-0.5 Å (blue wing, *left*) and with the 0.34 Å FWHM filter (21 March 2019) in Hα line core (*right*).

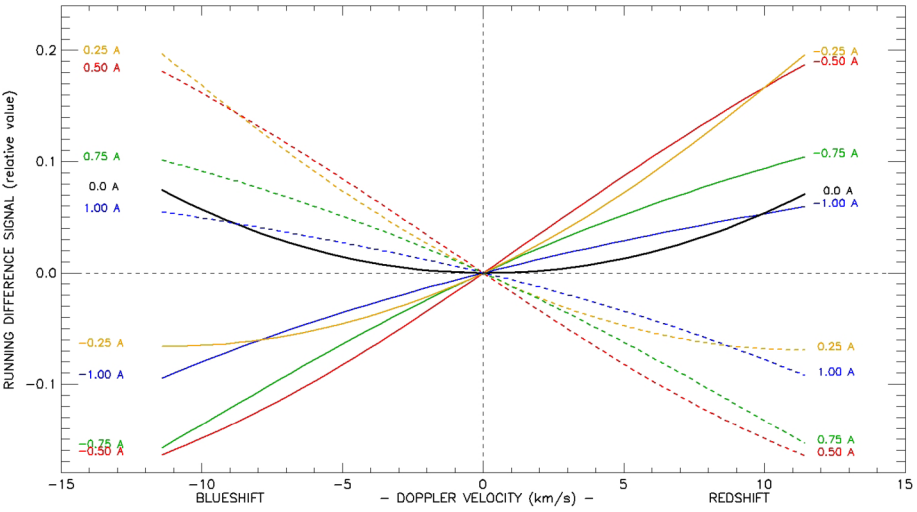

Figure 8 Running-difference signal as a function of Doppler velocity for different shifts of the filter bandpass (−1.0 to +1.0 Å by 0.25 Å step). *Solid lines*: blueshifted bandpass; *dashed lines*: redshifted bandpass. Bandpass shift: no shift (*black*), ±0.25 Å (*yellow*), ±0.50 Å (*red*), ±0.75 Å (*green*), ±1.0 Å (*blue*).

are convenient. These results are illustrated by movie 1 showing running differences of the 28 October 2003 event observed by the tunable Meudon Lyot filter (Hα center and wings).

As Moreton waves will probably not occur before the next maximum, a simulation of typical data which will be provided by the new instrument, based on 28 October 2003 data, is displayed in Figure 9. Real-time images and movies will be produced, as central intensities $I_c(t)$ or contrasts $C_c(t)$ and running differences of the blue wing intensity $I_b(t) - I_b(t-1)$ or contrast $C_b(t) - C_b(t-1)$. Contrasts give smoother results and are defined by $C = \frac{I}{LD} - 1$,

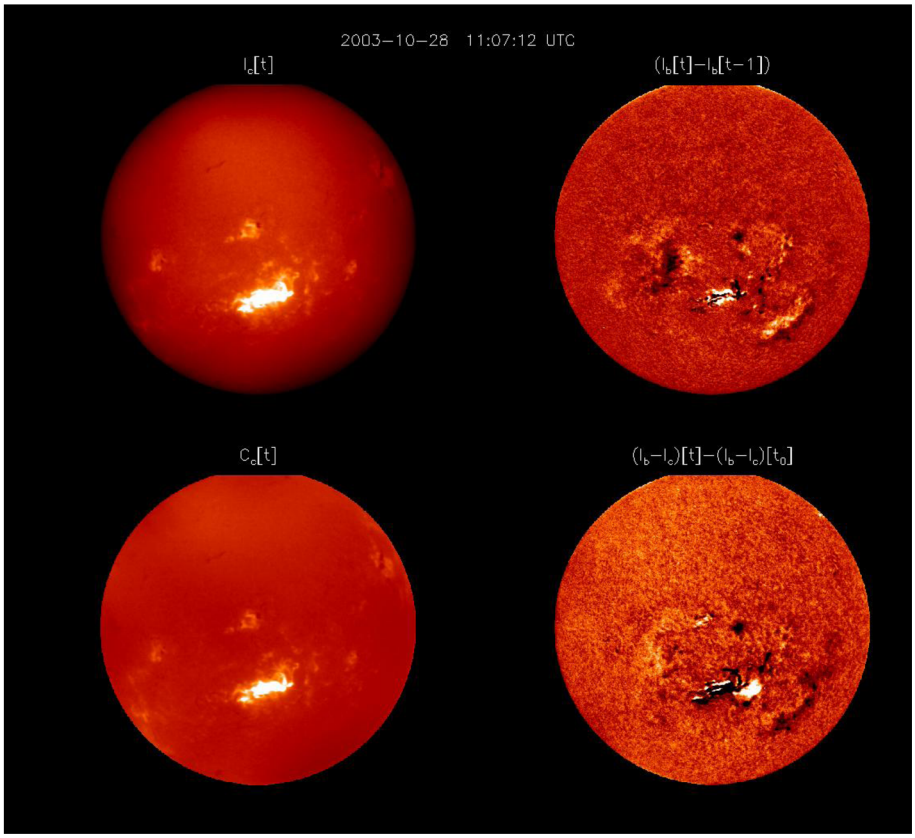

Figure 9 Simulation (based on the 28 October 2003 event at 11:07:12 UT) of data which will be produced by the new heliograph. *Top*: real-time images; central intensity (*left*) and running difference of the blue wing intensity (*right*). *Bottom*: post-processed images; contrast at line center suppressing the limb darkening (*left*) and Doppler proxy (*right*) issued from the intensity difference between the blue wing and line center, after correction by an offset observed before the event.

where LD is the limb darkening function. It is built from the image by taking median values in concentric rings.

Post-processed images will also be delivered. The two Hα filters can be combined to give $I'(t) = I_b(t) - I_c(t)$, I_b and I_c being, respectively, the blue wing and central intensity. Then an offset $I'(t_0)$, measured before the event, is subtracted to the current signal $I'(t)$, as suggested by Muhr *et al.* (2010). This provides a proxy of the Doppler velocity. Results issued from both wings would be better, but this cannot be done with our instrument. The method can be applied to contrasts instead of intensities, as shown by movie 2.

Hence, efforts to implement real-time detection of Moreton events using running differences of blue wing intensities are under way and will be refined using initial datasets from the instrument as it is commissioned. This tool, together with the survey of flare brightening in line core, could be used to monitor flare onset and anticipate their possible impact at the Earth.

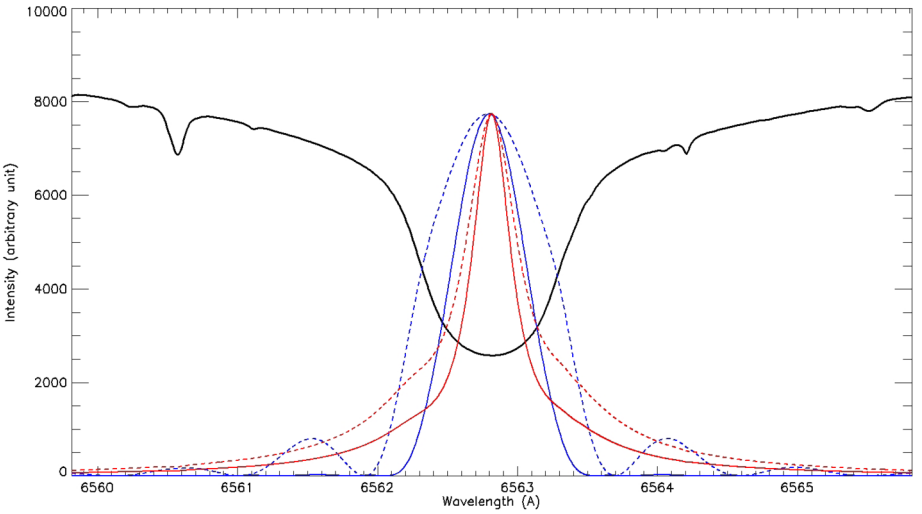

Figure 10 Spectral energy transmitted by old Hα Meudon Lyot prototypes (*blue*, 1985–2004 *solid*, 1965–1984 *dashed*) and the two DayStar Fabry–Pérot etalons (*red*, *solid* and *dashed*).

6. Discussion and Conclusion

More than 7 million images at 60 seconds cadence (flares, CME onset, filament instabilities, Moreton waves) have been obtained at Meudon and OHP from 1956 to 2004 using Hα Lyot filters, either line centered or three-wavelength (center + wings). Systematic observations will restart in 2020 at Calern observatory using more compact and cheaper technology. The new heliograph is based on two commercial Fabry–Pérot etalons. However, such filters have far photospheric wings (Lorentzian shape), contrarily to Lyot filters which mainly pass the chromosphere (Figure 10). Let us define the energy bandpass (EB) as the wavelength interval containing half of the energy transmitted by the filter. It is computed from the spectral energy (the product of the filter transmission curve by the quiet Hα disk center line profile). The EB of the Meudon three-wavelength Lyot filters (1965–1984 and 1985–1997), respectively 0.62 Å and 0.34 Å, is always smaller than their FWHM (the second filter was optically more optimized). In comparison, the distance between inflexion points of the Hα line is 1.0 Å. On the contrary, our industry Fabry–Pérot devices provide 0.53 Å and 0.77 Å EB, greater than their respective FWHM. Hence, more photospheric light will pass in comparison to previous Lyot prototypes, reducing for instance filament contrasts. However, adding 2.0 or 3.0 Å FWHM pre-filters would allow one, in the future, to minimize photospheric wing contributions and achieve former performance.

Three telescopes are available: high cadence (15 seconds) Hα center and blue wing, and medium cadence (60 s) CaII K (active regions and magnetic field proxy). Real-time and post-processed images for scientific purposes will be produced: Hα center for filament eruption and flare brightening detection, as well as running difference of blue wing for Moreton waves (often involved in large flares). All images (quick look JPEG and scientific FITS) will be freely available to the solar community through BASS2000, without any delay.

After 16 years of interruption (due to the lack of observers), this new automatic instrument will resume the exceptional survey started at the IGY. It will complete the GHN and GONG networks. GONG has only one european station in Tenerife. Weather conditions in

Côte d'Azur are the best available in France for continuous observations. This opportunity allows one to offer more time coverage to existing networks, improved cadence, core and wing observations. The new routine is dedicated to space weather scientific studies related to flares, CME and filament instabilities, as well as operational monitoring and forecast by the french Air Force. Detailed opto-mechanical drawings are available for reproduction at other places.

Acknowledgements We thank the anonymous referee for helpful comments and suggestions. We are indebted to the Meteospace technical team: G. Barbary, C. Blanchard, I. Bualé, S. Cnudde, C. Collin, C. Colon, D. Crussaire, A. Demathieu, C. Imad, Ph. Laporte, R. Lecocguen, M. Ortiz, Ch. Renié, D. Ziegler (Observatoire de Paris) and Y. Bresson, F. Guitton, F. Morand, C. Renaud (Observatoire de la Côte d'Azur). We are also grateful for financial support to the Direction Générale de l'Armement, the scientific councils of Paris and Nice Observatories, the IDEX UCA/JEDI académie 3, Ile de France régional council and the Programme National Soleil Terre (INSU/CNRS). K. Dalmasse is supported by the Centre National d'Etudes Spatiales (CNES).

Disclosure of Potential Conflicts of Interest The authors declare that they have no conflicts of interest.

Appendix: Electronic Supplemental Material (movies in MPEG 4 format)

i) Movie 1: Running difference of contrasts applied to the typical Moreton event of 28 October 2003 from 10:41 UT to 11:22 UT (Meudon Hα heliograph). Contrasts C are derived from intensities I after limb darkening (LD) correction ($C = \frac{I}{LD} - 1$). Time step 60 seconds. Top left: contrasts at line center; top right: running differences of line center contrasts; bottom: running differences of blue wing contrasts (Hα − 0.5 Å, left) and red wing contrasts (Hα + 0.5 Å, right).

ii) Movie 2: simulation of typical images and movies which will be provided by the new instrument, based on 28 October 2003 data, from 10:41 UT to 11:22 UT (Meudon heliograph). Top: real-time processing will provide running difference of contrasts (left) and intensities (right) in the blue wing (Hα - 0.5 Å). Contrasts C are derived from intensities I after limb darkening (LD) correction ($C = \frac{I}{LD} - 1$). Bottom: post-processing based on Muhr *et al.* (2010) method: base-difference between contrasts (left) or intensities (right) at time t and an offset measured before the event (reference time t_0), combining blue wing and line core images of the two Hα telescopes.

References

Amari, T., Luciani, J.F.: 1999, Confined disruption of a three-dimensional twisted magnetic flux tube. *Astrophys. J. Lett.* **515**(2), L81. DOI. ADS.

Antiochos, S.K., DeVore, C.R., Klimchuk, J.A.: 1999, A model for solar coronal mass ejections. *Astrophys. J.* **510**, 485. DOI. ADS.

Asai, A., Yokoyama, T., Shimojo, M., Masuda, S., Kurokawa, H., Shibata, K.: 2004, Flare ribbon expansion and energy release rate. *Astrophys. J.* **611**(1), 557. DOI. ADS.

Aulanier, G., Démoulin, P.: 1998, 3-D magnetic configurations supporting prominences. I. The natural presence of lateral feet. *Astron. Astrophys.* **329**, 1125. ADS.

Carmichael, H.: 1964, A process for flares. *NASA Spec. Publ.* **50**, 451. ADS.

Dalmasse, K., Chandra, R., Schmieder, B., Aulanier, G.: 2015, Can we explain atypical solar flares? *Astron. Astrophys.* **574**, A37. DOI. ADS.

Delbouille, L., Roland, G., Neven, L.: 1973, *Atlas Photométrique du Spectre Solaire de [lambda] 3000 à [lambda] 10000, Université de Liège*. ADS.
Demarcq, J., Olivieri, G., Fruteau de Laclos, M., Marteaud, M., Nicolas, M., Roussel, R.: 1985, A new instrument for solar observations. *L'Astronomie* **99**, 557. ADS.
Fletcher, L., Dennis, B.R., Hudson, H.S., Krucker, S., Phillips, K., Veronig, A., Battaglia, M., Bone, L., Caspi, A., Chen, Q., Gallagher, P., Grigis, P.T., Ji, H., Liu, W., Milligan, R.O., Temmer, M.: 2011, An observational overview of solar flares. *Space Sci. Rev.* **159**, 19. DOI. ADS.
Forbes, T.G., Priest, E.R.: 1984, Numerical simulation of reconnection in an emerging magnetic flux region. *Solar Phys.* **94**(2), 315. DOI. ADS.
Furth, H.P., Killeen, J., Rosenbluth, M.N.: 1963, Finite-resistivity instabilities of a sheet pinch. *Phys. Fluids* **6**(4), 459. DOI. ADS.
Gallagher, P.T., Denker, C., Yurchyshyn, V., Spirock, T., Qiu, J., Wang, H., Goode, P.R.: 2002, Solar activity monitoring and forecasting capabilities at big bear solar observatory. *Ann. Geophys.* **20**, 1105. DOI. ADS.
Grenat, H., Laborde, G.: 1954, Héliographe monochromatique de Lyot. *Ann. Astrophys.* **17**, 541. ADS.
Harvey, J.W., Bolding, J., Clark, R., Hauth, D., Hill, F., Kroll, R., Luis, G., Mills, N., Purdy, T., Henney, C., Holland, D., Winter, J.: 2011, Full-disk solar H-alpha images from GONG. In: *AAS/Solar Phys. Div. Abs. # 42*, *Bull. Am. Astron. Soc.* **43**, 17.45. ADS.
Hirayama, T.: 1974, Theoretical model of flares and prominences. I: evaporating flare model. *Solar Phys.* **34**, 323. DOI. ADS.
Isobe, H., Takasaki, H., Shibata, K.: 2005, Measurement of the energy release rate and the reconnection rate in solar flares. *Astrophys. J.* **632**(2), 1184. DOI. ADS.
Kahler, S.W., Moore, R.L., Kane, S.R., Zirin, H.: 1988, Filament eruptions and the impulsive phase of solar flares. *Astrophys. J.* **328**, 824. DOI. ADS.
Klassen, A., Aurass, H., Mann, G., Thompson, B.J.: 2000, Catalogue of the 1997 SOHO-EIT coronal transient waves and associated type II radio burst spectra. *Astron. Astrophys. Suppl. Ser.* **141**, 357. DOI. ADS.
Kliem, B., Török, T.: 2006, Torus instability. *Phys. Rev. Lett.* **96**(25), 255002. DOI. ADS.
Kopp, R.A., Pneuman, G.W.: 1976, Magnetic reconnection in the Corona and the loop prominence phenomenon. *Solar Phys.* **50**, 85. DOI. ADS.
Liu, R., Liu, C., Xu, Y., Liu, W., Kliem, B., Wang, H.: 2013, Observation of a Moreton wave and wave-filament interactions associated with the renowned X9 Flare on 1990 May 24. *Astrophys. J.* **773**(2), 166. DOI. ADS.
Lyot, B.: 1944, Le filtre monochromatique polarisant et ses applications en physique solaire. *Ann. Astrophys.* **7**, 31. ADS.
Maia, D., Aulanier, G., Wang, S.J., Pick, M., Malherbe, J.-M., Delaboudinière, J.-P.: 2003, Interpretation of a complex CME event: coupling of scales in multiple flux systems. *Astron. Astrophys.* **405**, 313. DOI. ADS.
Malherbe, J.-M., Dalmasse, K.: 2019, The new 2018 version of the Meudon spectroheliograph. *Solar Phys.* **294**(5), 52. DOI. ADS.
Martres, M.J.: 1989, The homologous flare events in solar active regions. *Solar Phys.* **119**, 357. DOI. ADS.
Martres, M.-J., Pick, M.: 1962, Matières propres aux eruptions chromosphériques associées à des emissions radio électriques. *Ann. Astrophys.* **25**, 293. ADS.
Masson, S., Pariat, E., Aulanier, G., Schrijver, C.J.: 2009, The nature of flare Ribbons in Coronal null-point topology. *Astrophys. J.* **700**, 559. DOI. ADS.
Michard, R.: 1965, Nouvel héliographe à l'Observatoire de Meudon. *L'Astronomie* **79**, 131. ADS.
Moore, R.L., Sterling, A.C., Hudson, H.S., Lemen, J.R.: 2001, Onset of the magnetic explosion in solar flares and coronal mass ejections. *Astrophys. J.* **552**, 833. DOI. ADS.
Moreton, G.E.: 1960, Hα observations of flare-initiated disturbances with velocities $\sim$1000 km/sec *Astron. J.* **65**, 494. DOI. ADS.
Mouradian, Z., Martres, M.J., Soru-Escaut, I.: 1983, The emerging magnetic flux and the elementary eruptive phenomenon. *Solar Phys.* **87**, 309. DOI. ADS.
Mouradian, Z., Soru-Escaut, I.: 1989, Role of rigid rotation in the sudden disappearance of solar filaments. *Astron. Astrophys.* **210**, 410. ADS.
Mouradian, Z., Soru-Escaut, I., Pojoga, S.: 1995, On the two classes of filament-prominence disappearance and their relation to coronal mass ejections. *Solar Phys.* **158**, 269. DOI. ADS.
Mouradian, Z., Martres, M.-J., Soru-Escaut, I., Simnett, G.M.: 1989, Comparison of Hα absorbing features with soft X-ray images at the onset of Solar Flares. *Astron. Astrophys.* **224**, 267. ADS.
Muhr, N., Vršnak, B., Temmer, M., Veronig, A.M., Magdalenić, J.: 2010, Analysis of a global Moreton wave observed on 2003 October 28. *Astrophys. J.* **708**(2), 1639. DOI. ADS.

Narukage, N., Hudson, H.S., Morimoto, T., Akiyama, S., Kitai, R., Kurokawa, H., Shibata, K.: 2002, Simultaneous observation of a Moreton wave on 1997 November 3 in Hα and soft X-rays. *Astrophys. J. Lett.* **572**(1), L109. DOI. ADS.

Nitta, N.V., Schrijver, C.J., Title, A.M., Liu, W.: 2013, Large-scale coronal propagating fronts in solar eruptions as observed by the atmospheric imaging assembly on board the solar dynamics observatory—an ensemble study. *Astrophys. J.* **776**(1), 58. DOI. ADS.

Pevtsov, A.A., Virtanen, I., Mursula, K., Tlatov, A., Bertello, L.: 2016, Reconstructing solar magnetic fields from historical observations. I. renormalized Ca K spectroheliograms and pseudo-magnetograms. *Astron. Astrophys.* **585**, A40. DOI. ADS.

Pick, M., Malherbe, J.-M., Kerdraon, A., Maia, D.J.F.: 2005, On the disk Hα and radio observations of the 2003 October 28 flare and coronal mass ejection event. *Astrophys. J. Lett.* **631**, L97. DOI. ADS.

Qiu, J., Lee, J., Gary, D.E., Wang, H.: 2002, Motion of flare footpoint emission and inferred electric field in reconnecting current sheets. *Astrophys. J.* **565**(2), 1335. DOI. ADS.

Schmieder, B., Forbes, T.G., Malherbe, J.M., Machado, M.E.: 1987, Evidence for gentle chromospheric evaporation during the gradual phase of large solar flares. *Astrophys. J.* **317**, 956. DOI. ADS.

Schmieder, B., Aulanier, G., Mein, P., López Ariste, A.: 2006, Evolving photospheric flux concentrations and filament dynamic changes. *Solar Phys.* **238**, 245. DOI. ADS.

Schrijver, C.J., Beer, J., Baltensperger, U., Cliver, E.W., Güdel, M., Hudson, H.S., McCracken, K.G., Osten, R.A., Peter, T., Soderblom, D.R., Usoskin, I.G., Wolff, E.W.: 2012, Estimating the frequency of extremely energetic Solar events, based on Solar, Stellar, Lunar, and Terrestrial records. *J. Geophys. Res.* **117**, 8103. DOI. ADS.

Shibata, K., Magara, T.: 2011, Solar flares: magnetohydrodynamic processes. *Living Rev. Solar Phys.* **8**, 6. DOI. ADS.

Soru-Escaut, I., Mouradian, Z.: 1990, Sudden disappearance and reappearance of solar filaments by heating and cooling. *Astron. Astrophys.* **230**, 474. ADS.

Sterling, A.C., Moore, R.L.: 2005, Slow-rise and fast-rise phases of an erupting solar filament, and flare emission onset. *Astrophys. J.* **630**(2), 1148. DOI. ADS.

Sturrock, P.A.: 1966, Model of the high-energy phase of Solar Flares. *Nature* **211**, 695. DOI. ADS.

Thompson, W.T.: 2006, Coordinate systems for solar image data. *Astron. Astrophys.* **449**(2), 791. DOI. ADS.

Toriumi, S., Schrijver, C.J., Harra, L.K., Hudson, H., Nagashima, K.: 2017, Magnetic properties of solar active regions that govern large solar flares and eruptions. *Astrophys. J.* **834**(1), 56. DOI. ADS.

Török, T., Kliem, B.: 2005, Confined and ejective eruptions of Kink-unstable flux ropes. *Astrophys. J. Lett.* **630**, L97. DOI. ADS.

Uchida, Y.: 1968, Propagation of hydromagnetic disturbances in the solar Corona and Moreton's wave phenomenon. *Solar Phys.* **4**(1), 30. DOI. ADS.

Warmuth, A.: 2015, Large-scale globally propagating coronal waves. *Living Rev. Solar Phys.* **12**(1), 3. DOI. ADS.